



# Spatial and temporal variability of rainfall in the Alps-Mediterranean Euroregion

Jean-François Rysman, Yvon Lemaître, Emmanuel Moreau

## ► To cite this version:

Jean-François Rysman, Yvon Lemaître, Emmanuel Moreau. Spatial and temporal variability of rainfall in the Alps-Mediterranean Euroregion. *Journal of Applied Meteorology and Climatology*, 2016, 55 (3), pp.655-671. 10.1175/JAMC-D-15-0095.1 . insu-01256555

**HAL Id: insu-01256555**

**<https://hal-insu.archives-ouvertes.fr/insu-01256555>**

Submitted on 9 Mar 2016

**HAL** is a multi-disciplinary open access archive for the deposit and dissemination of scientific research documents, whether they are published or not. The documents may come from teaching and research institutions in France or abroad, or from public or private research centers.

L'archive ouverte pluridisciplinaire **HAL**, est destinée au dépôt et à la diffusion de documents scientifiques de niveau recherche, publiés ou non, émanant des établissements d'enseignement et de recherche français ou étrangers, des laboratoires publics ou privés.

# Spatial and Temporal Variability of Rainfall in the Alps–Mediterranean Euroregion

JEAN-FRANÇOIS RYSMAN AND YVON LEMAÎTRE

*Université Pierre-et-Marie-Curie University of Paris 06, Paris, Université Versailles St-Quentin, Versailles, and  
CNRS/INSU, Laboratoire Atmosphères, Milieux, Observations Spatiales, Institut Pierre-Simon Laplace,  
Guyancourt, France*

EMMANUEL MOREAU

*Novimet, Guyancourt, France*

(Manuscript received 31 March 2015, in final form 23 December 2015)

## ABSTRACT

This study describes the main patterns of rainfall distribution in the Alps–Mediterranean “Euroregion” using a ground radar and characterizes the associated processes using model output. The radar dataset spans 2009–12 with fine spatial (1 km) and temporal (5 min) resolutions. The most significant rain accumulations were observed in 2009 and 2010, and the most intense extreme events occurred in 2010. Conversely, 2012 was a dry year. Model output revealed that the wind shear, the pressure, and the meridional wind at low level were the three main factors explaining the rainfall variability between 2009 and 2012. At the monthly scale, the maximum of rain accumulation was observed in November along the coast. Results also showed that the most intense rain rates were observed during early summer and autumn in the “Pre-Alps.” The monthly variability was characterized by a displacement of extreme rain events from land to sea from late spring to winter. Correlation analyses showed that this displacement was essentially controlled by the convective available potential energy (CAPE). Rainfall showed a diurnal variability from April to August for the land areas of the Alps–Mediterranean Euroregion. The diurnal variability was significant during the spring and summer months, with maximal rain intensity between 1600 and 1800 UTC. The correlation of the rainfall with CAPE showed that this cycle was related to atmospheric instability. A secondary peak in average rain rate was observed during the early morning and was likely triggered by land breezes. The results highlighted that rainfall characteristics are extremely diverse in terms of intensity and distribution in this relatively small region.

## 1. Introduction

Precipitation is spread unevenly, both spatially and temporally, in the Mediterranean Sea region (Funatsu et al. 2009; Nastos et al. 2013). Its areal distribution is controlled by both small-scale and large-scale processes. At the large scale, the Mediterranean region is affected both by midlatitude cyclones and subtropical highs (Lionello et al. 2006). The midlatitude cyclones favor precipitation during winter, whereas the subtropical high pressure centers (e.g., Azores high) inhibit precipitation during the summer. Additional large-scale features such as the North Atlantic Oscillation (NAO) and El Niño–Southern Oscillation (ENSO) impact the

intensity and distribution of the rain (Price et al. 1998; Mariotti et al. 2002b; Haylock and Goodess 2004; Karagiannidis et al. 2008; Boccolari and Malmusi 2013). At the regional scale, local forcings such as topography (e.g., the southern part of the Alps) affect the atmospheric circulation that impacts the average rainfall distribution (Smith et al. 2003; Walser and Schar 2004; Panziera and Germann 2010).

During the past few years, heavy-precipitation events have had an impact on the Mediterranean region, resulting in damaging floods, notably in Vaison-la-Romaine, France, in September 1992 (Sénési et al. 1996); Izmir, Turkey, in November 1995 (Kömüşçü 1998); Algiers, Algeria, in November 2001 (Argence et al. 2008); and Gard, France, in September 2002 (Delrieu et al. 2005; Ducrocq et al. 2008). These events caused numerous casualties (e.g., 886 casualties for the Algiers event), and the damage cost billions of euros. Consequently, there is a

---

*Corresponding author address:* Jean-François Rysman, LATMOS, 11 Boulevard d’Alembert, 78280 Guyancourt, France.  
E-mail: rysman@latmos.ipsl.fr

growing interest in understanding and forecasting rainfall distribution and, in particular, intense events, because they often have devastating consequences on both society and the economy.

This study focuses more specifically on the Alps–Mediterranean “Euroregion” that was recently impacted by several devastating floods such as in Draguignan, France (15–16 June 2010; [Fresnay 2014](#)); Nice (France)–Genoa (Italy) (1–6 November 2011; [Silvestro et al. 2012](#); [Rebora et al. 2013](#)); and Cannes, France (4 October 2015). In more general terms, meteorological weather services reported 110 heavy-rain events in this region during the period of focus of this study from 2009 to 2012 (European Severe Weather Database; [Dotzek et al. 2009](#)). Most of these events occurred along the coast and in the Alps during autumn. Twenty-two casualties associated with heavy precipitation were reported, and 20 of them were associated with the Draguignan event. The heaviest events occurred during 2010: on 15 June 2010 in Draguignan [ $220 \text{ mm (24 h)}^{-1}$ ] and Hyères, France [ $178 \text{ mm (12 h)}^{-1}$ ]; 8 September 2010 in Pegli, Italy [ $124 \text{ mm (2 h)}^{-1}$ ]; and 4 October 2010 in Pegli [ $373 \text{ mm (24 h)}^{-1}$ ] and Piampaludo, Italy [ $291 \text{ mm (24 h)}^{-1}$ ]. All of these examples illustrate the need to better understand and forecast rainfall in this particular region.

The Alps–Mediterranean Euroregion is characterized by two major geographical features: the southern part of the Alps (Maritime Alps) and a small portion of the northwestern Mediterranean Sea. The southern part of the Alps is prone to heavy precipitation because of its proximity to the Mediterranean Sea and its steep topography. Moreover, it is characterized by numerous river catchments that respond quickly to heavy rainfall, leading to frequent flash floods. In this region, rain is mainly measured using a rain gauge network that has an average spatial resolution of  $5 \text{ km} \times 5 \text{ km}$ , but it is highly heterogeneous (isolated valleys are not equipped), is not intercalibrated, and has only an hourly or a daily temporal resolution. In addition, the rain gauges collect rain on a surface of a few centimeters square that is not necessarily representative of the volume of water at the surface of a  $5 \text{ km} \times 5 \text{ km}$  area. Nevertheless, accurate understanding and forecasting of rain processes over this region require homogeneous measurements of precipitation at finescale. Indeed, using nonhydrostatic numerical models, [Walser and Schar \(2004\)](#) highlighted the very low predictability for some convective rainfall even in catchments as big as  $50\,000 \text{ km}^2$  in this region. [Smith et al. \(2003\)](#) showed that the rainfall field depends on some local-scale characteristics down to  $10 \text{ km}$ . A fine temporal scale is also needed, since thunderstorms can trigger events with a considerable accumulation of rain

but with a typical life time of 30 min ([Orlanski 1975](#); [Atkinson 1981](#)).

The rain characteristics over the Mediterranean Sea are little known. In this region, the precipitation is mainly estimated using satellite measurements (e.g., [Mariotti et al. 2002a](#); [Funatsu et al. 2009](#); [Claud et al. 2012](#); [Tapiador et al. 2012](#); [Nastos et al. 2013](#)) and instrumented buoys (e.g., [Nittis et al. 2007](#)). The former provide a large range of information but with coarse spatial and temporal resolutions, typically  $0.5^\circ \times 0.5^\circ$  and 6 h. The latter provide in situ rain measurements but with sparse spatial coverage. Yet, it is important to obtain accurate and dense rain measurements over this region because precipitation modifies the sea surface temperature, which affects exchanges between the sea and the atmosphere that in turn impact atmospheric processes. It is also worth recalling that the evaporation from the Mediterranean Sea accounts for 40%–60% of the water vapor feeding the heavy convective systems in the southeastern part of France ([Duffourg and Ducrocq 2011, 2013](#)), indicating its major impact on the climate of the Alps–Mediterranean Euroregion.

In this context, an X-band radar (8–12 GHz) named Hydrix has been in place since 2008 in the central part of the Alps–Mediterranean Euroregion to quantify and understand the hydrological cycle and related processes. This radar offers spatial and temporal resolutions of  $1 \text{ km}^2$  and 5 min, respectively, and thus provides fine-scale and homogeneous information about the rainfall behavior of this region. Few radar studies of long-term rain observations in mountainous regions are available to date (e.g., [Wüest et al. 2010](#); [Rudolph et al. 2011](#)). This is mainly because of logistical and signal-treatment issues. The logistical problems are related to the installation and maintenance of radars in hard-to-access regions. This problem is reduced with X-band radars, which have a small antenna size (1.5 m for Hydrix antenna) in comparison with C-band or S-band radars (4–8 and 2–4 GHz, respectively). The signal-treatment issue is mainly related to ground clutter in mountainous regions. This difficulty was partially overcome with the development of Doppler and polarimetric capacities, which offer improved detection of ground clutter. The use of the X-band frequency rather than C and S bands also improves the contrast between meteorological targets and ground clutter ([Testud et al. 2007](#)). Moreover, in the case of the Hydrix radar, the offset antenna reduces the level of sidelobes, which also improves radar visibility.

The present work uses this radar to characterize the precipitation that occurs in the Alps–Mediterranean Euroregion. The objective is to describe the main patterns of rainfall distribution as well as their associated

processes. Moreover, this study aims to discover whether the variability of these patterns and their associated processes depends on temporal scales and/or on local characteristics. Specifically, this study analyzes the large-scale temporal variability (2009–12) of rainfall as well as its monthly and diurnal variability in several subregions as detailed in [section 3](#). Rainfall accumulation and extreme-rainfall events are investigated. Moreover, to understand the rainfall variability and the underlying mechanisms, statistical analyses of correlation between rain and meteorological parameters at annual, monthly, and diurnal scales have been conducted. Such information is of high relevance to better understanding the processes associated with rainfall in the Mediterranean, leading to improved forecasts. It will also contribute to answering key scientific questions addressed in the international Hydrological Cycle in Mediterranean Experiment (HyMeX) project ([Drobinski et al. 2008, 2014](#)) such as the characterization of extreme hydrometeorological events in the Mediterranean [Working Group 3 (WG3) scientific question 1 (SQ1)] and the improvement of heavy-rainfall process knowledge and prediction (WG3-SQ2).

The simultaneous finescale analysis of rainfall over several regions with very different characteristics (e.g., mountain or sea) is new. Whereas numerous studies analyze rainfall behavior at a single scale, this study takes advantage of the fine resolution and the long-standing database to highlight properties of rainfall from small to large temporal scales. Moreover, the homogeneity of the database is ensured by using one single-radar instrument to measure rainfall, as opposed to multiple rainfall collectors. Also, most regional-scale studies identify the processes associated with rainfall by using several case studies, whereas this study aims to identify these processes statistically.

This paper is organized as follows. [Section 2](#) presents some technical information about the Hydrix radar and the model output. In [section 3](#), we present the region studied and the methods. [Section 4](#) is dedicated to the results: from the large scale (4-yr variability) to the small temporal scale (diurnal cycle). The discussion and conclusions are given in [section 5](#).

## 2. Radar characteristics

The main characteristics of the Hydrix radar are summarized in [Table 1](#). This X-band and polarimetric radar measures reflectivity at five elevations from  $-1^\circ$  to  $4^\circ$ . The ZPHI (named after the reflectivity  $Z$  and the differential phase shift  $\Phi_{DP}$ ) algorithm ([Testud et al. 2000](#)) converts radar reflectivity into rainfall intensity. This algorithm corrects the signal from beam attenuation

TABLE 1. Main characteristics of the Hydrix radar. Here, H and V indicate horizontal and vertical, respectively, and rpm indicates revolutions per minute.

Frequency (GHz)	9.3
Peak power (kW)	35 per channel
Antenna (m)	1.5 (offset feed)
Antenna gain (dB)	$\geq 41$
Beamwidth ( $^\circ$ )	1.5
Sidelobe level (dB)	$\leq -30$
Pulse width (ns)	500–2000
Pulse repetition frequency (Hz)	1000–500
Sensitivity (dBZ)	0 at 70 km
Polarization mode	Simultaneous H and V
Scan speed ( $^\circ \text{ s}^{-1}$ )	14 (2.3 rpm)
Revisit time (min)	5

along each radial and computes the  $N_0^*$  parameter of the drop size distribution  $N(d)$  (see [Testud et al. 2000](#)) to retrieve the rain rate  $R$  using the

$$R = a(N_0^*)^{1-b} Z^b \quad (1)$$

relationship, where  $R$  is the rain rate, and  $a$  and  $b$  are two constant empirical coefficients. As a result, the ZPHI algorithm takes into account the drop size distribution variability to estimate rainfall rate. The rainfall rate initially estimated in polar coordinates is then projected onto an extended Lambert II Cartesian grid. A horizontal interpolation is performed using the Cressman method, with a 1.33-km cutoff length (i.e., the 0.66-km Cressman radius, which has been shown to be optimal for a  $1\text{-km}^2$  grid) for  $1\text{ km} \times 1\text{ km}$  resolution. Then, the surface rain rate is estimated using a weighted average of the rainfall obtained at multiple altitudes. Weights are a function of the altitude of the measurements; the precipitation type—notably snow, hail, or liquid;<sup>1</sup> and the beam masking [see also [Le Bouar et al. \(2008\)](#), [Moreau et al. \(2009\)](#), and [Rysman \(2013\)](#)]. The bright band is detected in the classification processing chain using both model prediction (as a first guess when available) and polarimetric observations as  $\rho_{mv}$ . When the radar only samples snow, a  $Z$ – $R$  relationship is used to convert reflectivity to equivalent liquid precipitation. Evaluations of retrieved rainfall using this radar and the associated ZPHI algorithm were performed using S-band radar observations ([Diss et al. 2009](#)) and rain gauge measurements ([Moreau et al. 2009](#); [Rysman 2013](#)). They showed that the quality of the rainfall data is generally good, but it is sometimes low in the northern part of the radar domain for distances larger than 100 km

<sup>1</sup> The precipitation type is inferred using a fuzzy-logic classification that takes advantage of polarization.

from the radar and in the whole of the Po region (except for the coastline). For this reason, in this study we excluded this region and measurements taken farther away than 100 km from the radar.

The rainfall database extends almost continuously from March 2009 until 2012. The spatial resolution is  $1 \text{ km}^2$ , and the temporal resolution is 5 min. The high spatial and temporal resolutions and the range of measurements offer worthwhile opportunities to study the rain characteristics in the region (see, e.g., [Rysman et al. 2013](#); [Lemaître et al. 2013](#)).

### 3. Region studied and methods

The radar is located on the top of a mountain called Mont Vial (1550 m) close to Nice. The area covered by the Hydrix radar range encompasses Provence in France to the Po region in Italy from west to east (see [Fig. 1](#), top panel). The northern domain of the radar encompasses the southern part of the Alps (France's Ubaye–Orrenaye region), whereas the southern radar domain includes a small part of the northern Mediterranean Sea.

The regional topography strongly affects the rainfall distribution and intensity in the Alps–Mediterranean Euroregion, as shown in [Frei and Schär \(1998\)](#). Therefore, the region is divided for the analyses into five distinct subregions on the basis of generalized geophysical properties ([Fig. 1](#), bottom panel). These subregions are a plain (Provence) with a maximal altitude of 500 m; the Maritime Alps (Alps) with a minimal altitude of 1400 m; the “Pre-Alps” with altitudes ranging from 500 to 1400 m, the coast, which includes land and sea to a maximum of 15 km from the coastline; and the Mediterranean Sea.

In this study, we used outputs from the Weather Research and Forecasting (WRF) Model ([Skamarock et al. 2008](#)) to analyze statistically the factors that affect the precipitation in the Alps–Mediterranean Euroregion. In particular, we used a hindcast simulation that covers the European and Mediterranean region from January 1989 to November 2011. This simulation was achieved within the framework of the Mediterranean domain of the Coordinated Regional Climate Downscaling Experiment (MED-CORDEX; [Giorgi et al. 2009](#)) and HyMeX ([Drobinski et al. 2014](#); [Ducrocq et al. 2014](#)) projects. The spatial resolution was 20 km, and outputs were stored every 3 h. Initial conditions and boundary conditions were obtained using the ERA-Interim reanalysis from the European Centre for Medium-Range Weather Forecasts ([Simmons et al. 2007](#); [Dee et al. 2011](#)). In the vertical direction, 28 unevenly spaced levels are used and the atmosphere top is at 50 hPa. Topography data originate from 5-min-resolution U.S. Geological Survey data. Soil type is based on a combination of the 10-min

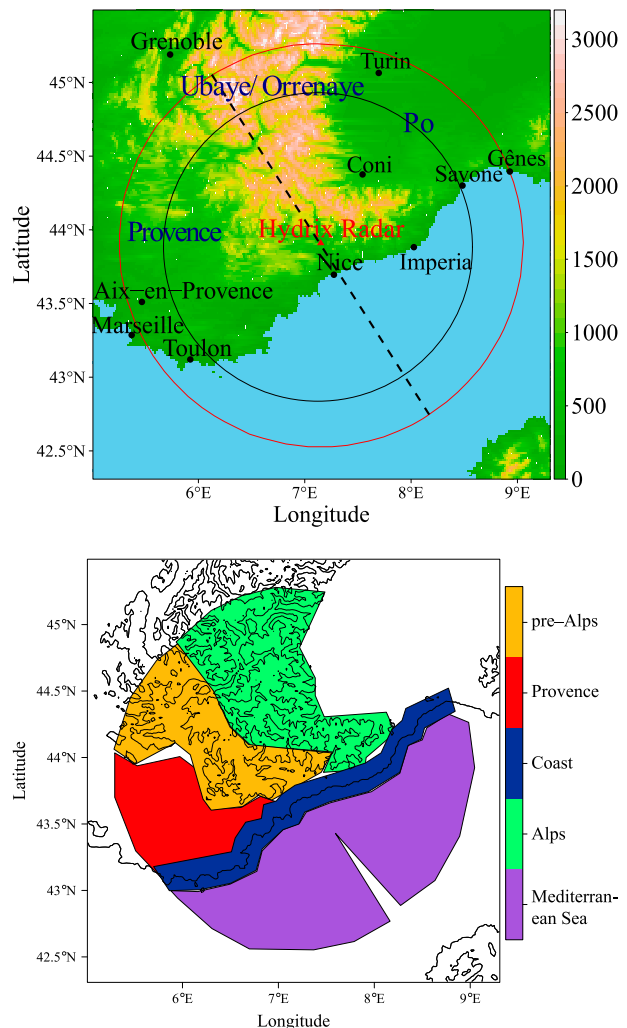


FIG. 1. (top) Hydrix radar maximum range (outer red circle) and accurate rainfall estimation range (inner black circle); the ground elevation (m) is displayed in color. Main cities are indicated in black and regions are indicated in blue. The  $x$  axes of the Hovmöller diagrams in [Fig. 2](#) (below) are along the black dashed line. (bottom) The five subregions studied: Pre-Alps, Provence, coast, Alps, and the Mediterranean Sea.

17-category United Nations Food and Agriculture Organization soil data and the U.S. State Soil Geographic 10-min soil data. The parameterizations used include the WRF single-moment five-class microphysical parameterization ([Hong et al. 2004](#)), the new Kain–Fritsch convective parameterization ([Kain 2004](#)), the Dudhia shortwave radiation ([Dudhia 1989](#)) and Rapid Radiative Transfer Model longwave radiation ([Mlawer et al. 1997](#)), the Yonsei University planetary boundary layer scheme [Noh et al. \(2003\)](#), and the Rapid Update Cycle land surface model ([Smirnova et al. 1997, 2000](#)). The WRF simulation has been relaxed toward the ERA-Interim large-scale fields with a nudging time of 6 h.



With this set of parameterizations, water content is exchanged among water vapor, cloud water, cloud ice, snow, and rain. It allows for mixed-phase processes, supercooled water, and snowmelt in addition to ice sedimentation. CAPE is computed using the thermodynamical profiles. Further information about the simulations can be obtained from Stéfanon et al. (2013) and Berthou et al. (2014).

We correlated rainfall measured by the radar with some relevant parameters of the model to identify the factors that affect the precipitation. Case studies performed in neighboring regions (Boudevillain et al. 2009; Nuissier et al. 2008; Ricard et al. 2012; Duffourg and Ducrocq 2011) had identified meteorological parameters that appeared to be associated with precipitation. These same parameters are the ones considered in this statistical analysis: pressure  $P$ , potential vorticity  $PV$ , specific humidity  $q$ , divergence and convergence of specific humidity flux [ $\text{div}(vq)$  and  $\text{conv}(vq)$ ], wind direction (with north indicated as N, east given as E, south indicated as S, and west denoted by W), wind divergence  $\text{div}(v)$  and convergence  $\text{conv}(v)$ , convective available potential energy CAPE, and wind shear from 0 to 6 km WS.

To identify nonlinear correlations, we used the Spearman correlation coefficient. Correlation coefficients higher (lower) than 0.1 ( $-0.1$ ) are statistically significant (permutation test: number of permutations  $i = 10\,000$ , sample size  $n = 500$ , and  $p$  value = 0.01). This statistical analysis provided a huge quantity of significant and complex correlations depending on altitude, location, and season. The full description of these correlations is beyond the scope of this paper [for details see Table A1 in the appendix and also Rysman (2013)]. Therefore, in this paper, we focus on significant correlations that might explain the observed interannual, monthly, and diurnal variability of precipitation.

## 4. Results

### a. 4-yr variability

The first aspect explored in this paper is the large-temporal-scale variability of the rain intensity and distribution from 2009 to 2012. To this end, we computed Hovmöller diagrams and ensured that their spatial axes were perpendicular to the coastline, that is, in the southeast–northwest direction (see Fig. 1, top panel).

Maximum daily rain accumulations were in general found from October to April, and minima were found during the summer (July–August) with significant interannual variability (Fig. 2a). The maxima were mainly located along the coast except for January 2012 when

the maximum of rain accumulation shifted into the Mediterranean Sea region. The maxima occurred during autumn 2010 and in January 2012, with rain accumulations higher than  $4.5 \text{ mm day}^{-1}$ . The intensity of the maxima varied strongly from one year to another (e.g., autumn 2009 vs autumn 2010). The summers of 2011 and 2012 were very dry, with nearly no rain in July 2012. The ERA-Interim reanalysis for rainfall in the Alps–Mediterranean showed that 2010 was the third rainiest year in the 1979–2012 period and that the 2009–12 period was slightly (i.e., 9%) rainier than the average of 1979–2012.

A cross correlation for time-lag zero was computed for the atmospheric parameters discussed in the previous section to understand the large-scale variability of rainfall observations. Rainfall and parameters were averaged in the radar domain. In the following, we have only presented the results for parameters for which the cross correlations were significant: potential vorticity in the high troposphere  $PV_t$ , potential vorticity in the midtroposphere  $PV_m$ , meridional wind in the low troposphere  $v_b$ , specific humidity in the low troposphere  $q_b$ , high-tropospheric pressure  $P_t$  (note that cross correlation is quasi independent of altitude for pressure), CAPE, and WS. The results in Fig. 3 should be understood as follows: when a given parameter is significantly cross correlated with rainfall and rainfall shows either a positive or negative anomaly, it implies that the rainfall anomaly is associated with the parameter.

The meteorological parameters that explained the large-scale pattern of rainfall anomalies were wind shear, high-tropospheric pressure, and meridional wind at low levels. In particular, the positive rainfall anomalies of January–March 2010, October–December 2010, March 2011, and November 2011 appeared to be strongly influenced by these three factors. For the November 2011 case, the humidity at low levels also played a role in the positive rainfall anomaly.

It is not surprising that high-tropospheric pressure, wind shear, and meridional wind at low levels play a significant role in rainfall anomalies at the large scale, because these factors are associated with frontal perturbation. In particular, meridional wind is strong ahead of frontal systems that bring humidity over the Alps–Mediterranean Euroregion. Wind shear is also strong ahead of frontal systems while pressure is low. It is interesting to note that, although CAPE is correlated with rainfall during the summer, this parameter does not explain rainfall anomalies for the large temporal scales.

The extreme rain events that occurred during the 2009–12 period in the Alps–Mediterranean Euroregion are shown in Fig. 2b. The rainfall extremes are defined as the 99.9999th quantile (Q99) of the rain probability distribution function (PDF). To be specific, we computed

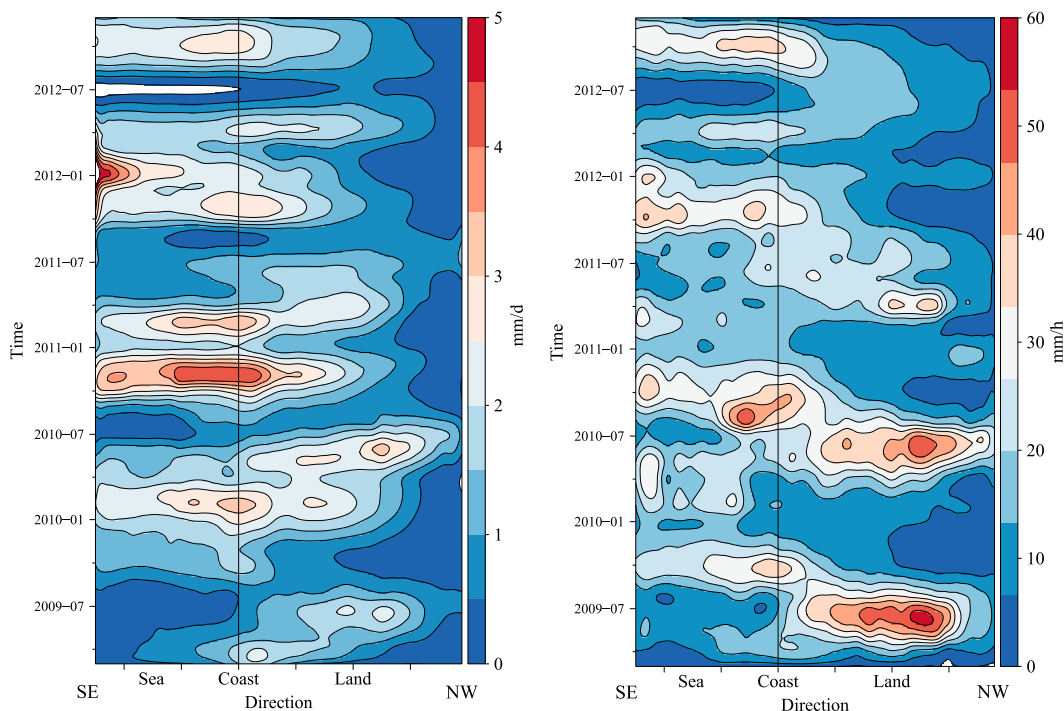


FIG. 2. Hovmöller diagrams computed along the black dashed line shown in Fig. 1 (perpendicular to the coast) for (left) daily radar rain accumulation ( $\text{mm day}^{-1}$ ) and (right) Q99 of radar rain rate ( $\text{mm h}^{-1}$ ). Q99 is defined as the rain rate below which 99.9999% of the estimated rain rates are found. The vertical black line symbolizes the coast.

the PDF of the 5-min rain rate ( $\sim 1 \times 10^9$  rain-rate estimations per subregion and per month) and extracted the rain-rate value for which 99.9999% of the estimated rain rates were lower. A pronounced seasonal cycle was

observed for the extreme event. The most striking pattern was the displacement of the extreme events from land to sea between late spring and winter. The 4-yr variability of extreme events was high: the intensity of

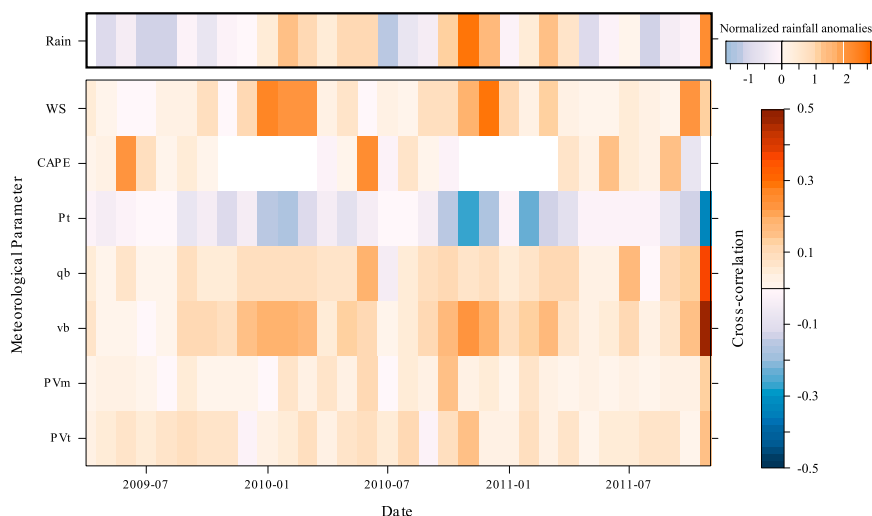


FIG. 3. Normalized (scaled and centered) monthly area-mean radar rainfall anomalies and the cross correlation between monthly rainfall and meteorological parameters (PVt, PVm, vb, qb, Pt, CAPE, and WS, as defined in the text) for time-lag zero as a function of the month. Blue (orange) corresponds to a negative (positive) anomaly for rainfall and a negative (positive) cross correlation for other meteorological parameters.

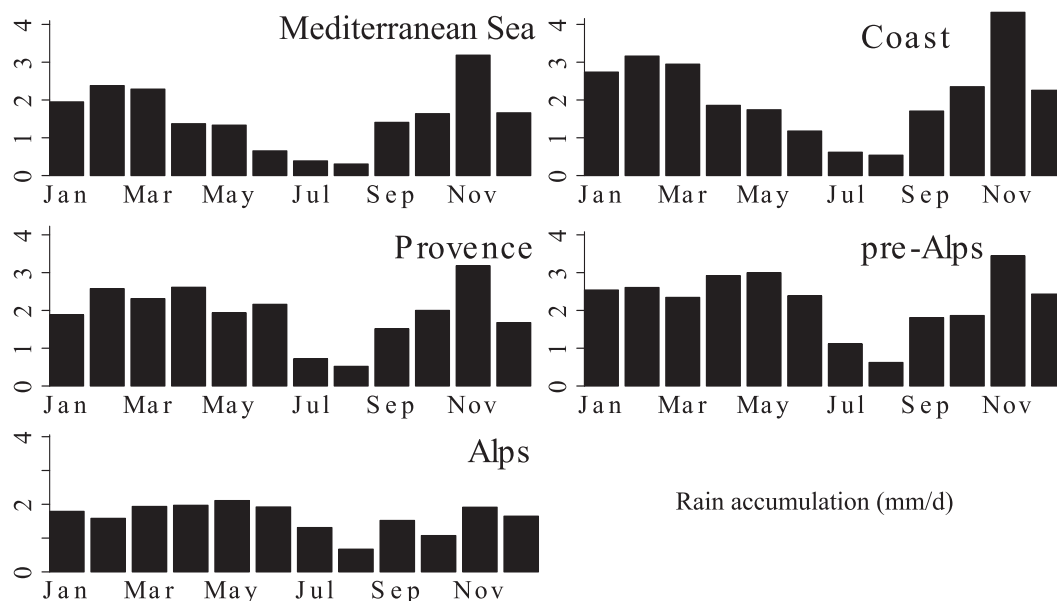


FIG. 4. Bar plot of daily radar rain accumulation ( $\text{mm day}^{-1}$ ) averaged per month and per region.

the late-spring maxima decreased between 2009 ( $>60 \text{ mm h}^{-1}$ ) and 2011 ( $\sim 35 \text{ mm h}^{-1}$ ). In 2012 no late-spring maximum was observed. The maximum over the sea during autumn occurred every year but varied in intensity and was higher in 2010 ( $\sim 50 \text{ mm h}^{-1}$ ) than in other years ( $\sim 35 \text{ mm h}^{-1}$ ). In general, the position of the maxima was constant year after year, except during spring 2012. Note that the maximum observed in June 2010 was partly related to the Dragunian event.

### b. Seasonal cycle

Several authors have identified a strong monthly variability of rainfall in the Mediterranean basin (Frei and Schär 1998; Funatsu et al. 2009; Nastos et al. 2013). In this section, we characterize this variability at the regional scale for daily rain accumulation and extreme rain events.

#### 1) DAILY RAIN ACCUMULATION

The daily rainfall accumulation per month exhibited very contrasting behavior both spatially and temporally (Fig. 4). Three distinct patterns were thus observed: the first for the sea and the coast, the second for the Pre-Alps and Provence, and the third for the Alps.

The first pattern was characterized by a maximum rainfall accumulation in November,  $4.3 \text{ mm day}^{-1}$  for the coast and  $3.2 \text{ mm day}^{-1}$  for the Mediterranean Sea, and a substantial rainfall accumulation from January to March ( $2\text{--}3 \text{ mm day}^{-1}$ ). In detail, the rainfall accumulation slowly decreased from winter to summer and reached its minimum in August ( $<0.3 \text{ mm day}^{-1}$  for the

Mediterranean Sea and  $0.5 \text{ mm day}^{-1}$  for the coast). Then the rainfall accumulation increased strongly in September and October ( $1.8\text{--}2.2 \text{ mm day}^{-1}$ ) and reached a maximum in November. Note that rainfall accumulation was nearly 2 times as high in November as in the previous and following months (October and December).

The second pattern was characterized by two quasi-equal maxima of rainfall accumulation in April (Provence)/May (Pre-Alps) and in November ( $2.6\text{--}3.1 \text{ mm day}^{-1}$ ). In detail, the average rainfall accumulation increased slowly from January to April (Provence)/May (Pre-Alps) and then decreased until August ( $0.5\text{--}0.6 \text{ mm day}^{-1}$ ). Then it increased gradually until November.

The third pattern, observed for the Alps region, showed weak monthly variability and low rainfall accumulation ( $\sim 1.6 \text{ mm day}^{-1}$ ) during the whole year. In detail, the average rainfall accumulation increased slightly from January ( $1.8 \text{ mm day}^{-1}$ ) to May ( $2.1 \text{ mm day}^{-1}$ ). During the second part of the year the rainfall accumulation oscillated between  $0.7 \text{ mm day}^{-1}$  in August and  $1.9 \text{ mm day}^{-1}$  in November without any obvious tendency.

Figure 4 highlights the small-scale variability of rainfall accumulation over the region but also the strong regional dependency of rain. For example, in June the rainfall accumulation was lower than  $1 \text{ mm day}^{-1}$  over the Mediterranean but higher than  $2 \text{ mm day}^{-1}$  over Provence, located a few kilometers to the north. The results also highlight a rain accumulation that was significantly higher in November than in the other months.



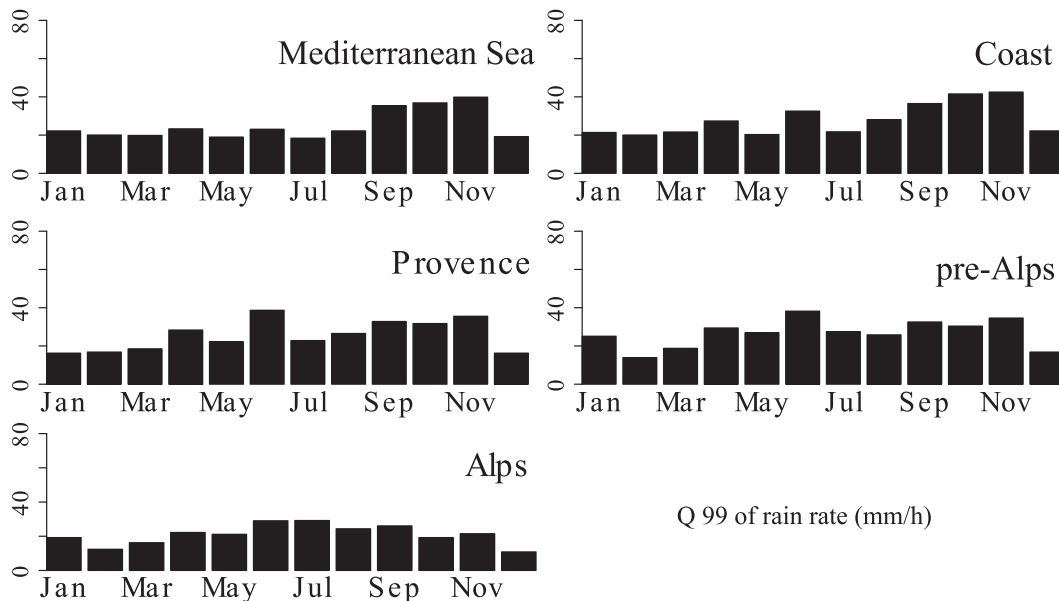


FIG. 5. Bar plot of Q99 of radar rain rate ( $\text{mm h}^{-1}$ ) per region and per month.

The reason is first that during autumn there are a lot of atmospheric perturbations that travel across this region, contrary to the summer season when anticyclonic conditions are present (Lionello et al. 2006). These atmospheric perturbations are thus propitious for heavy rainfall (Funatsu et al. 2008). Moreover, during summer, the Mediterranean Sea warms up and gains a lot of energy that is released during autumn when the temperature of the Mediterranean Sea is higher than the land (Mariotti et al. 2002a; Ducrocq et al. 2014). As a result, rain accumulation is higher in November than in other autumn months, probably because conditions are optimal during this month: the Mediterranean Sea is still warm and there are many atmospheric fronts that travel over the region. Our results are consistent in terms of location and rain amount with those obtained from rain gauge measurements reported by Frei and Schär (1998).

## 2) EXTREME RAIN EVENTS

Regarding the extreme rain events (Fig. 5), three distinct types of behavior were also observed. First, the coast and the Mediterranean Sea showed a moderate seasonal cycle: the extreme rain rate was nearly constant between December and August, ranging from 19 to 23  $\text{mm h}^{-1}$ . From September to November the rain rate was much more significant (35–40  $\text{mm h}^{-1}$ ).

For the Pre-Alps and Provence the highest rain rates were observed in June (38  $\text{mm h}^{-1}$  for the Pre-Alps and 39  $\text{mm h}^{-1}$  for Provence). Conversely, the rain rate was low between December and March (16–25  $\text{mm h}^{-1}$ ). It increased from April (28–29  $\text{mm h}^{-1}$ ) to June and then

decreased slightly from July to November (35–36  $\text{mm h}^{-1}$ ). The pattern for the Alps region was similar to the previous pattern except that the peak in June was less significant (29  $\text{mm h}^{-1}$ ) and the rain rate decreased strongly from June to December (only 11  $\text{mm h}^{-1}$ ).

Note that the distribution of extreme events differs from Fig. 4, meaning that the extreme events are not the only contributors to rain accumulation. This is particularly true in November when rain accumulation is very high (especially for the coast) while the rain rate associated with heavy-precipitation events is moderate. It means that during this period some long-lasting events with moderate rain rates occurred. These types of events can also be associated with considerable flooding since they feed the rivers continuously for long periods (see, e.g., the recent events in the Gard region during autumn 2014).

As already highlighted in Fig. 2b, these results show that the rain maxima tend to move from land to sea during the year: during spring and the beginning of summer, the most extreme precipitation was observed inland (Provence, Pre-Alps, and Alps), whereas during the autumn months the most extreme precipitation was mainly located over the coast and the sea. It is not surprising to find the most extreme events in the Pre-Alps region since this region is characterized by steep topography and is close to the sea. These two factors are known to be favorable for the development of intense convective cells and substantial rain rates in the western Mediterranean region (Ducrocq et al. 2014).

As for the 4-yr variability, numerous correlation analyses were performed to identify the parameters (and

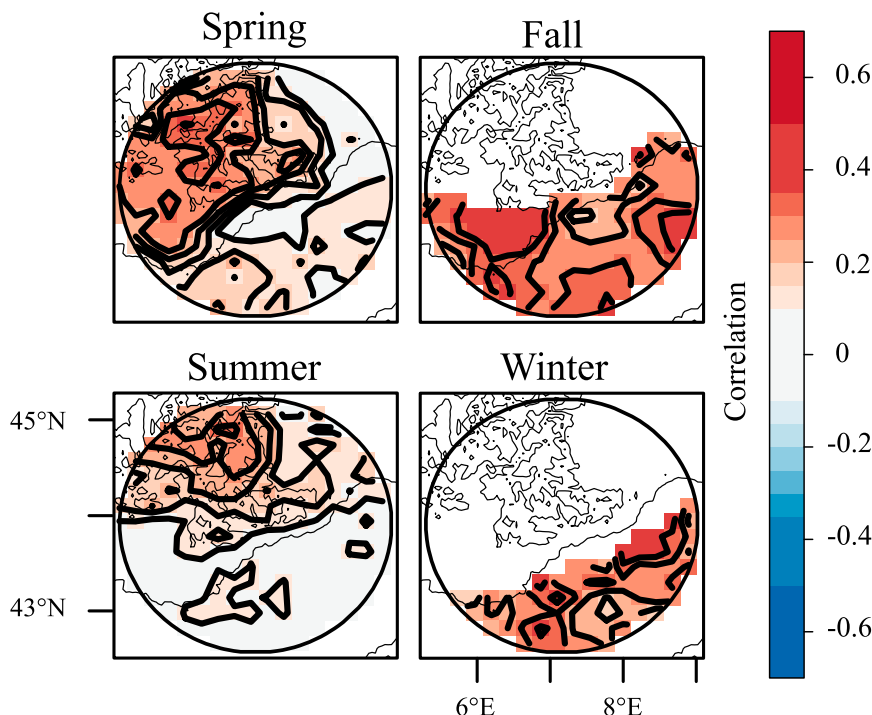


FIG. 6. Spearman correlation between 3-h rainfall from radar measurements interpolated on the WRF 20-km grid and CAPE per season. Red or blue indicates a positive or negative correlation, respectively.

underlying processes) that drive the monthly pattern of rainfall in the Alps–Mediterranean Euroregion. Among the various parameters considered (not shown), CAPE appeared to explain most of the rain displacement. Figure 6 shows that the correlation between rainfall (from radar measurements interpolated on the WRF 20-km grid) and CAPE during spring was fair (0.2–0.5) over land and weak or zero over sea. During the summer, the correlation was moderate (0.2–0.3) over alpine regions and was zero everywhere else. During the autumn and winter seasons, the correlation was strong over the sea (0.2–0.4) and weak over land except over Provence where correlation was strong (0.4) during autumn.

This correlation pattern explains the displacement of rainfall maxima from land to sea between spring and autumn. During autumn and winter, CAPE is low or zero over land while being significant over the sea. CAPE provides energy to convective motions that trigger rainy events over the sea. During the spring and summer, the situation is more complex, since CAPE is substantial over both land and sea (not shown) but the correlation is high only over land. This behavior is probably related to the absence of regional-scale lifting mechanisms needed to release CAPE over the sea. Indeed, during summer, anticyclonic conditions dominate in the Mediterranean region (Lionello et al. 2006),

restricting vertical motions. Therefore, no large-scale processes lift air masses to the level of free convection, preventing convective motions over the sea. Over land, alternative lifting processes are available such as orographic and thermal lifting.

The land–sea displacement was noticed in the past, at a more global scale, by Frei and Schär (1998) and by Funatsu et al. (2009) and has occurred in the whole of the northern part of the Mediterranean region [see Fig. 2 in Nastos et al. (2013)]. Yet, this is the first time, to our knowledge, that it has been shown to be tightly related to convective precipitation.

### c. Diurnal variability

The objective of this last section is to characterize the diurnal cycle of precipitation and to identify associated processes. The diurnal cycle is the strongest over land during spring, with a maximum in the average rain rate in the afternoon (Fig. 7). In addition, a secondary peak is observed in the early morning in the coastal and Mediterranean regions in August, September, and November. In greater detail, in January and February the diurnal signal was weak or absent for all regions. During this period, rainfall was maximal for the coast and the Mediterranean Sea ( $\sim 0.15 \text{ mm h}^{-1}$ ). In March a slight peak in the afternoon was observed for the coast,

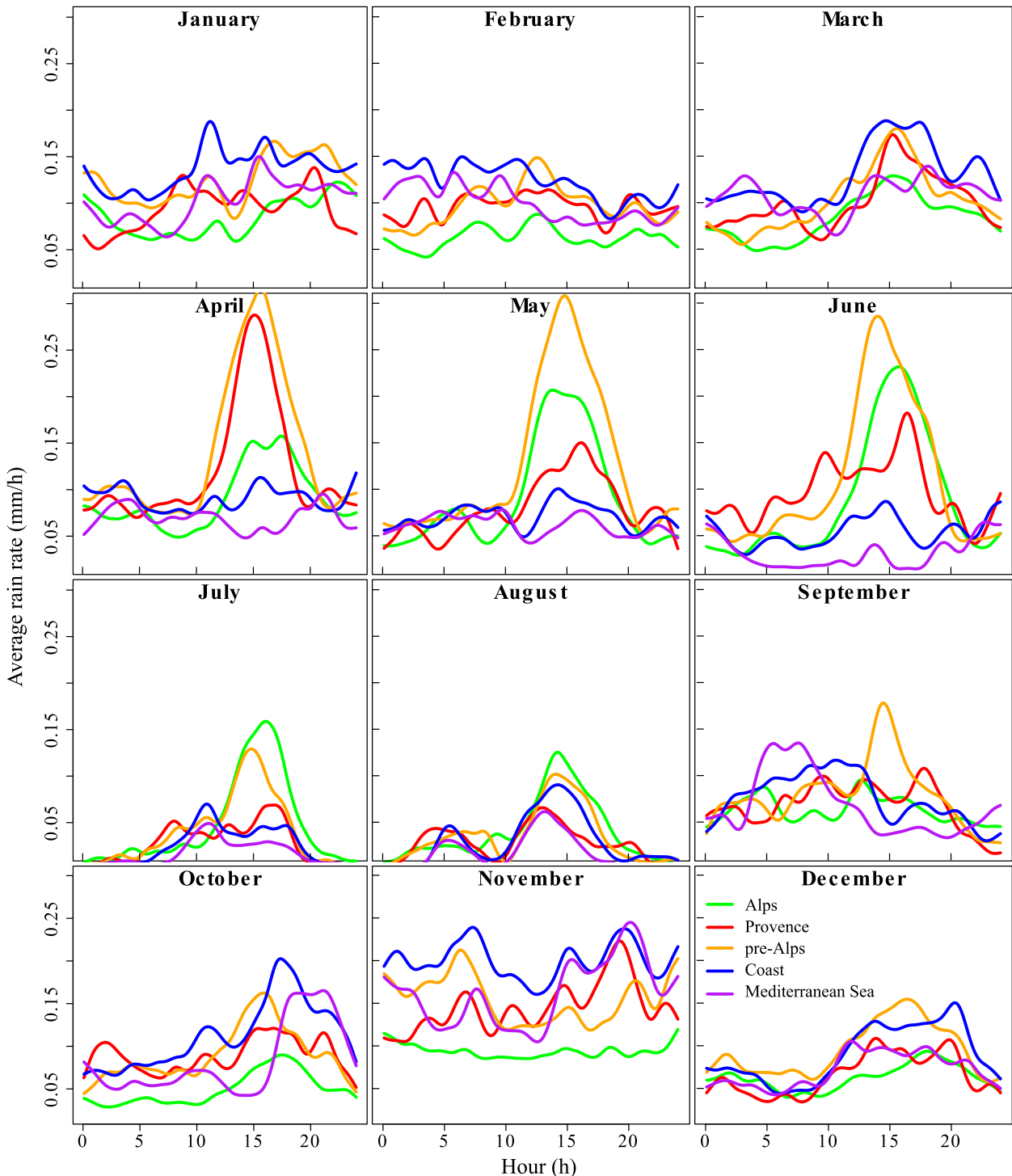


FIG. 7. Average diurnal cycle of radar rain rate ( $\text{mm h}^{-1}$ ) per region and per month.

Provence, and the Pre-Alps. This peak was much more significant in April, especially in the Pre-Alps and Provence regions (peak of  $0.32 \text{ mm h}^{-1}$  at 1600 UTC). In May and June a diurnal signal was observed in all land

regions and was maximal in the Pre-Alps ( $\sim 0.30 \text{ mm h}^{-1}$ ; 1500 UTC). From July, the diurnal signal became weaker (e.g., afternoon peak of  $0.16 \text{ mm h}^{-1}$  in the Alps and  $0.13 \text{ mm h}^{-1}$  in the Pre-Alps). In August, the diurnal

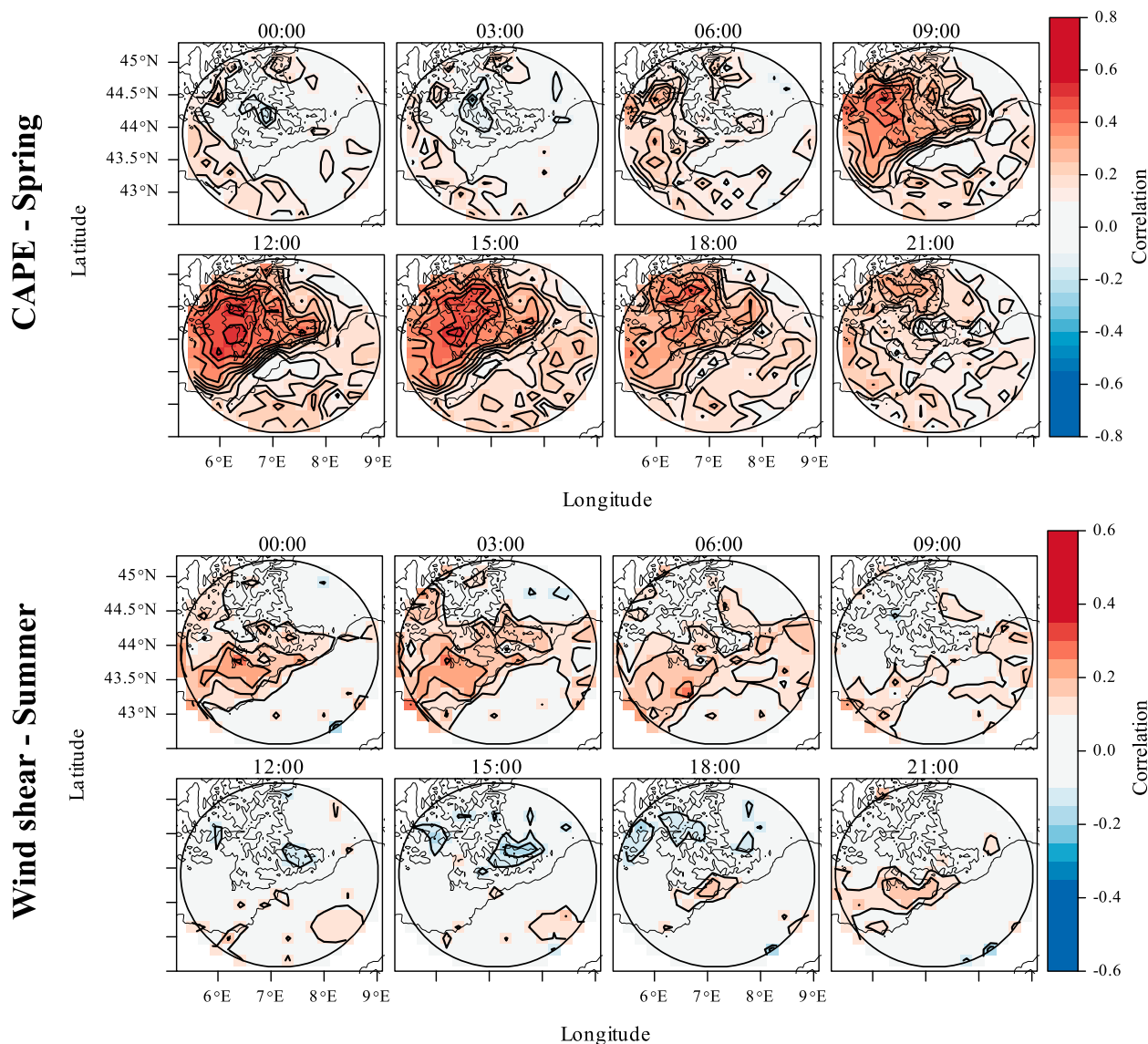


FIG. 8. Correlation between 3-h rainfall from the radar measurements interpolated on the WRF 20-km grid and (top) CAPE during spring and (bottom) wind shear during summer. Positive (negative) correlations are in red (blue).

signal was very weak and the average rain rate was the lowest of the year ( $<0.13 \text{ mm h}^{-1}$  everywhere). In September and October there was no clear diurnal signal, except for the Pre-Alps and coast regions, and the average rain rate was  $0.09 \text{ mm h}^{-1}$  (September) and  $0.12 \text{ mm h}^{-1}$  (October). In November the average rain rate was the highest of the year (up to  $0.23 \text{ mm h}^{-1}$  for the coast). A slight increase in rain rate could be seen during the afternoon for Provence, the coast, and the Mediterranean Sea. In December the overall rain rate was low and a slight diurnal signal existed for the coast, the Pre-Alps, and the Mediterranean Sea.

Using spatial correlation analysis, we identified the two main parameters from those previously indicated

that are associated with the diurnal cycle: CAPE and wind shear (Fig. 8). Correlation is displayed for spring for CAPE and for summer for wind shear, because the associated diurnal signal was maximal during these seasons. For CAPE, the correlation was significant (higher than 0.2) from 0900 to 2100 UTC, with a maximum correlation between 1200 and 1500 UTC (up to 0.8). Spatially, the maxima of correlation were observed over land and in particular over the Pre-Alps. From 0000 to 0600 UTC a very slight correlation existed without a clear spatial pattern. Thus, CAPE explained the afternoon peak in the diurnal cycle of land regions.

For wind shear (Fig. 8, bottom panel), the correlation was significant from 0000 to 0600 UTC (approximately

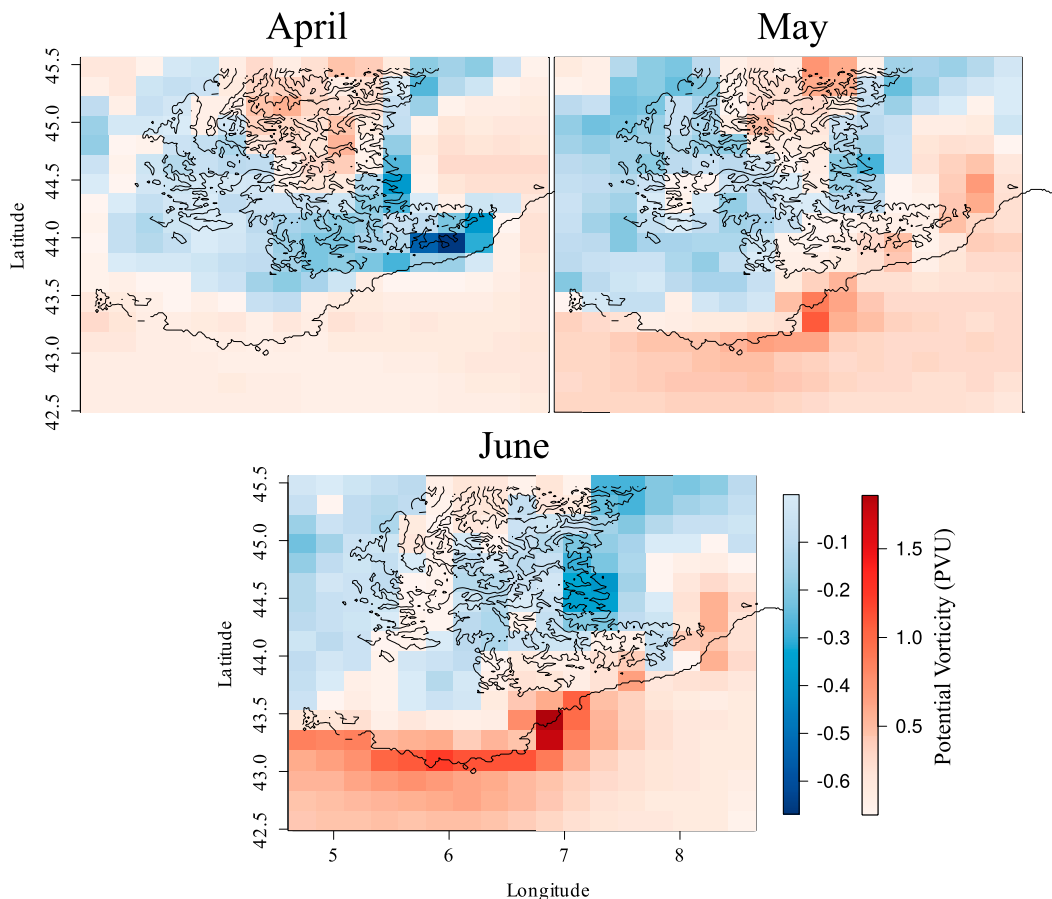


FIG. 9. Median of potential vorticity (PVU;  $1 \text{ PVU} = 10^{-6} \text{ K m}^2 \text{ kg}^{-1} \text{ s}^{-1}$ ) at 1000 hPa for April, May, and June. Blue (red) shows a negative (positive) potential vorticity, i.e., an unstable (a stable) lower atmosphere.

0.2). The maximum correlation was observed for the coastal region up to 30 km inland while no correlation was observed over the sea. Thus, the wind shear might explain the secondary peak observed in the early morning in coastal and Mediterranean regions in August, September, and November in Fig. 7. Similar peaks in the early morning have already been noticed for various regions in the world: in California (Landin and Bosart 1989), in Japan (Oki and Musiak 1994), and in Scotland (Svensson and Jakob 2002). Some of the previously mentioned authors argued that this behavior might be related to both the cooling of air over land during the night and a land-breeze convergence along the coast. The correlation analysis (Fig. 8) tends to support this explanation as the land breeze triggers air circulation from land to sea close to the ground and from sea to land in the mid- to high troposphere (i.e., a vertical wind shear).

Overall, the observed diurnal cycle and the correlation analyses highlight two main mechanisms that drive the precipitation during the year. During spring and

summer, the average rainfall rate shows a strong peak in the afternoon but is low during the night and early morning, and precipitation is driven by CAPE (Fig. 8, top panel). Therefore, during these seasons, rainfall appears to be mainly driven by short and convective rainfall. Conversely, during autumn and winter, the rainfall is spread throughout the day without a strong maximum, and no local correlation was highlighted. Therefore, the rainfall appears to be mainly driven by large-scale frontal perturbations that trigger weak and long-lasting stratiform precipitation.

Looking in more detail at the regional behavior of diurnal cycles, in Fig. 7 we also see that, in April, the diurnal signal is strong in the Pre-Alps and Provence regions but weak in the Alps. Moreover, from May to July, the diurnal signal in Provence becomes gradually weaker while the diurnal signal in the Alps gains in strength. This behavior could be partially related to the low-level stability of these regions. This stability can be highlighted using the potential vorticity (Fig. 9). A negative (positive) potential vorticity at ground level



highlights an unstable (stable) atmosphere. Thus, in April, the potential vorticity at ground level is negative over Provence and the Pre-Alps but is positive over the Alps. Later, in May and June, the potential vorticity over the Alps becomes progressively negative. Therefore, convective activity is more likely earlier in the season for regions with low altitudes (Provence) and is more likely later in the season for regions with high altitudes (the Alps). The decrease of the diurnal signal in Provence from spring to summer could be related to anticyclonic conditions found during the summer months (Lionello et al. 2006). These conditions tend to inhibit convection and could explain why the diurnal signal is weaker during this season in Provence. Other land regions present higher diurnal signals during this season, probably because they have a steeper orography, which is more favorable to convective activity since it provides the necessary lifting to release the convective instability.

The diurnal cycle highlighted here can be compared with results of Mandapaka et al. (2012) (Switzerland) and Gladich et al. (2011) (Italy). The region studied by Mandapaka et al. (2012) corresponds to the central Alps and can be mainly compared with the Alps region of our study. Similar to our results, Mandapaka et al. (2012) revealed a significant peak in rain accumulation of approximately  $0.2 \text{ mm h}^{-1}$  during the summer from 1000 to 0000 UTC. During other seasons, the diurnal cycle is flat and the average value is  $\sim 0.05 \text{ mm h}^{-1}$ , again similar to our results. They also showed that the diurnal cycle in the central Alps is mainly related to the local orographic forcing. Gladich et al. (2011) studied a region in southeastern Italy that is very similar to the Alps–Mediterranean Euroregion. They highlighted an increase in rainfall accumulation from 0900 UTC to 0000 UTC in annual average in this region (peak value of  $0.25 \text{ mm h}^{-1}$ ) that is similar to our results. In addition, they highlighted two distinct peaks during the day (1300 and 2100 UTC) that we did not observe.

## 5. Discussion and conclusions

This study analyzed the variability of rainfall distribution and intensity in the Alps–Mediterranean Euroregion using a 4-yr rainfall time series. Rainfall was measured by an X-band polarimetric and Doppler radar named Hydrix that is located close to the city of Nice in France. This radar provides a unique dataset with fine spatial (1 km) and temporal (5 min) resolutions and encompasses five subregions with very different geophysical characteristics: Provence, the Maritime Alps, the Pre-Alps, the coast, and the Mediterranean Sea.

Rainfall variability was described from large (4-yr variability) to small (diurnal variability) temporal scales.

Maxima of rain daily accumulation were observed during autumn 2010 and in January 2012 along the coast and over the sea. The most intense extreme events were observed during summer 2009 in the northern part of the study region (i.e., the Alps). The interannual variability was moderate for daily rain accumulation and high for extreme-rain events. Correlation analyses showed that rainfall positive anomalies during the 4-yr period were triggered by favorable conditions of wind shear, pressure, and meridional wind.

The monthly variability of rainfall was highly dependent on regional characteristics. In particular, three different behaviors were identified: the first for the sea and the coast, the second for the Pre-Alps and Provence, and the third for the Alps. The highest rain accumulation was observed for the coast in November ( $4.3 \text{ mm day}^{-1}$ ), and the lowest rain accumulation was observed for the Mediterranean Sea in August ( $<0.3 \text{ mm day}^{-1}$ ). The most intense extreme events were observed in June in the Pre-Alps and Provence regions. This analysis highlights a displacement of extreme-rainfall events from land to sea during the year, and correlation analyses show that this displacement is associated with the convective activity that moves from land during spring and summer to the sea during autumn [see, e.g., autumn 2012 in Rysman et al. (2016)].

The diurnal cycle is significant from April to August in land regions. In particular, the highest rain accumulations occur between 1000 and 2000 UTC and are related to convective processes, as shown by the high correlation between rainfall and CAPE. A secondary peak in the diurnal cycle is also detected in the early morning for regions close to the sea during autumn and winter. This is probably the signature of a land-breeze convergence along the coast.

Overall, this analysis provides an overview of rainfall characteristics in a complex region from fine to large temporal scales. One of the main findings is that rainfall variability is surprisingly high in this relatively small region. This variability is highly dependent on surface conditions (e.g., see the different behavior between the coast and Provence or the Pre-Alps) as well as the temporal scales considered. Representing this high variability in models is challenging, and resolution on the scale of a kilometer appears to be a minimum in this region.

While several case studies have identified the main parameters associated with the rainfall in neighboring regions, this study identified statistically the parameters that explain most of this rainfall variability from large to small scales. First, results show that the parameters governing rainfall variability depend on the scale considered. At the climatological scale, rainfall appears to be mainly driven by parameters that are the signatures



TABLE A1. Correlation coefficients between rainfall and meteorological parameters as a function of altitude and season.

	div( $uq$ )	conv( $uq$ )	PV	$P$	div( $v$ )	conv( $v$ )	E	W	N	S	$q$	CAPE	WS
High troposphere													
Winter	−0.08	0.14	0.31	−0.33	−0.01	0.16	−0.01	0.07	0.20	−0.11	−0.23		
Spring	−0.07	0.12	0.17	−0.20	0.01	0.07	−0.07	—	0.19	−0.06	−0.07		
Summer	−0.15	0.15	0.29	−0.48	0.01	0.17	0.16	−0.18	0.31	−0.17	−0.33		
Autumn	−0.21	−0.04	0.31	−0.41	−0.09	0.06	0.07	−0.14	0.20	−0.27	−0.26		
Midtroposphere													
Winter	0.08	0.23	0.14	−0.32	0.11	−0.01	0.00	0.19	0.24	−0.07	0.26		
Spring	0.09	0.16	0.03	−0.18	0.03	−0.03	0.01	−0.13	0.29	−0.04	0.30		
Summer	0.16	0.34	0.14	−0.47	0.23	−0.01	0.17	0.31	0.46	−0.11	0.34		
Autumn	0.16	0.35	0.25	−0.40	0.14	−0.07	0.04	0.08	0.38	−0.24	0.46		
Low troposphere													
Winter	0.07	0.13	0.11	−0.32	0.11	0.04	0.05	0.21	0.22	−0.03	0.18		
Spring	0.04	0.09	−0.02	−0.17	0.04	−0.03	0.07	−0.02	0.29	−0.05	0.27		
Summer	0.15	0.25	0.09	−0.47	0.22	−0.03	0.14	0.30	0.44	−0.08	0.34		
Autumn	0.18	0.35	0.21	−0.40	0.09	−0.04	0.07	0.15	0.42	−0.12	0.50		
Other													
Winter												0.18	0.11
Spring												0.12	0.08
Summer												0.28	0.29
Autumn												0.26	0.31

of frontal systems (north wind; low pressure). At the meteorological scale, CAPE and wind shear appear to be key parameters statistically. This is not surprising because theoretical studies have shown that both parameters are known to strongly influence convective systems (Rotunno and Klemp 1982; Rotunno et al. 1988; Weisman and Rotunno 2000). Because these parameters are highly dependent on finescale conditions, however, their accurate representation is difficult. This is probably why numerical weather models have not been as good as extrapolation forecasts in predicting precipitation patterns up to 3–4 h, although the former represent the atmospheric physics better (Lin et al. 2005; Vasić et al. 2007; Panziera et al. 2011).

This study identifies several parameters associated with rainfall, but there is a need for a better understanding of the reason for such a close relationship between rainfall and these parameters, that is, to identify the mechanisms leading to rainfall. It is also important to understand the behavior of these parameters better—for example, what governs the displacement of CAPE during the year and why the atmosphere is unstable in Provence from April and later in the Alps.

The results of this study can be used to evaluate the representation of the observed variability by regional models. In particular, similar statistics, such as the analysis of rainfall at several scales and the study of each component of rainfall (accumulation, extreme, etc.), could be conducted using rainfall simulated by the WRF Model or other models in the same region. Also, this radar system will continue to provide rainfall measurements that will allow us to study climatic tendencies in the Alps–Mediterranean

Euroregion. In particular, within the framework of climate change, it is extremely important to be able to detect an aridification of the region and/or an increase in the occurrence and frequency of extreme rainfall (Ban et al. 2015) so as to adapt our society's habits.

**Acknowledgments.** We acknowledge Georges Scialom and Céline Bellard for their perspicacious comments and for the careful proofreading of this paper. We also acknowledge Sophie Bastin and Marc Stéfanon for providing us with simulation outputs and diagnostics and Chantal Claud for her support that allowed us to achieve this work. The authors thank the three anonymous reviewers whose valuable feedback improved the paper. This study was sponsored by the École Doctorale 129—Sciences de l'environnement, the Direction Générale de l'Armement (PRECIP-CLOUD project), and by the ANR-REMEMBER. This work is a contribution to the HyMeX program through INSU/MISTRALS support and the MedCORDEX program, with access granted to the HPC resources of IDRIS (under Allocation i2011010227). The NCAR Command Language (version 6.2.1; Brown et al. 2012) was used for CAPE computation, and R software (<http://www.R-project.org/>) was used for other analyses.

## APPENDIX

### Details of the Rainfall Correlations

Table A1 provides a summary of the correlation coefficients between rainfall and meteorological parameters as a function of altitude and season in the study area.

## REFERENCES

- Argence, S., D. Lambert, E. Richard, J.-P. Chaboureaud, and N. Söhne, 2008: Impact of initial condition uncertainties on the predictability of heavy rainfall in the Mediterranean: A case study. *Quart. J. Roy. Meteor. Soc.*, **134**, 1775–1788, doi:10.1002/qj.314.
- Atkinson, B., 1981: *Meso-Scale Atmospheric Circulations*. Academic Press, 495 pp.
- Ban, N., J. Schmidli, and C. Schär, 2015: Heavy precipitation in a changing climate: Does short-term summer precipitation increase faster? *Geophys. Res. Lett.*, **42**, 1165–1172, doi:10.1002/2014GL062588.
- Berthou, S., S. Mailler, P. Drobinski, T. Arsouze, S. Bastin, K. Béranger, and C. Lebeaupin-Brossier, 2014: Prior history of mistral and tramontane winds modulates heavy precipitation events in southern France. *Tellus*, **66A**, 24064, doi:10.3402/tellusa.v66.24064.
- Boccolari, M., and S. Malmusi, 2013: Changes in temperature and precipitation extremes observed in Modena, Italy. *Atmos. Res.*, **122**, 16–31, doi:10.1016/j.atmosres.2012.10.022.
- Boudevillain, B., and Coauthors, 2009: Projet CYPRIM, partie I: Cyclogenèses et précipitations intenses en région méditerranéenne: Origines et caractéristiques (CYPRIM project, part I: Cyclogenesis and intense precipitation in the Mediterranean region: Origins and characteristics). *Meteorologie*, **66**, 18–28, doi:10.4267/2042/28828.
- Brown, D., R. Brownrigg, M. Haley, and W. Huang, 2012: The NCAR Command Language (NCL) (version 6.0.0). UCAR/NCAR Computational and Information Systems Laboratory, doi:10.5065/D6WD3XH5.
- Claud, C., B. Alhammoud, B. M. Funatsu, C. Lebeaupin Brossier, J.-P. Chaboureaud, K. Béranger, and P. Drobinski, 2012: A high resolution climatology of precipitation and deep convection over the Mediterranean region from operational satellite microwave data: Development and application to the evaluation of model uncertainties. *Nat. Hazards Earth Syst. Sci.*, **12**, 785–798, doi:10.5194/nhess-12-785-2012.
- Dee, D. P., and Coauthors, 2011: The ERA-Interim reanalysis: Configuration and performance of the data assimilation system. *Quart. J. Roy. Meteor. Soc.*, **137**, 553–597, doi:10.1002/qj.828.
- Delrieu, G., and Coauthors, 2005: The catastrophic flash-flood event of 8–9 September 2002 in the Gard region, France: A first case study for the Cévennes Vivarais Mediterranean Hydrometeorological Observatory. *J. Hydrometeorol.*, **6**, 34, doi:10.1175/JHM-400.1.
- Diss, S., J. Testud, J. Lavabre, P. Ribstein, E. Moreau, and J. Parent du Chatelet, 2009: Ability of a dual polarized X-band radar to estimate rainfall. *Adv. Water Resour.*, **32**, 975–985, doi:10.1016/j.advwatres.2009.01.004.
- Dotzek, N., P. Groenemeijer, B. Feuerstein, and A. M. Holzer, 2009: Overview of ESSL's severe convective storms research using the European Severe Weather Database ESWD. *Atmos. Res.*, **93**, 575–586, doi:10.1016/j.atmosres.2008.10.020.
- Drobinski, P., and Coauthors, 2008: HyMeX—Towards a major field experiment in 2010–2020: White book. Météo-France—Centre National de Recherches Météorologiques Tech. Rep., 124 pp. [Available online at [http://www.hymex.org/public/documents/WB\\_1.3.2.pdf](http://www.hymex.org/public/documents/WB_1.3.2.pdf).]
- , and Coauthors, 2014: HyMeX: A 10-year multidisciplinary program on the Mediterranean water cycle. *Bull. Amer. Meteor. Soc.*, **95**, 1063–1082, doi:10.1175/BAMS-D-12-00242.1.
- Ducrocq, V., O. Nuissier, D. Ricard, C. Lebeaupin, and T. Thouvenin, 2008: A numerical study of three catastrophic precipitating events over southern France. II: Mesoscale triggering and stationarity factors. *Quart. J. Roy. Meteor. Soc.*, **134**, 131–145, doi:10.1002/qj.199.
- , and Coauthors, 2014: HyMeX-SOP1: The field campaign dedicated to heavy precipitation and flash flooding in the northwestern Mediterranean. *Bull. Amer. Meteor. Soc.*, **95**, 1083–1100, doi:10.1175/BAMS-D-12-00244.1.
- Dudhia, J., 1989: Numerical study of convection observed during the Winter Monsoon Experiment using a mesoscale two-dimensional model. *J. Atmos. Sci.*, **46**, 3077–3107, doi:10.1175/1520-0469(1989)046<3077:NSOCOD>2.0.CO;2.
- Duffourg, F., and V. Ducrocq, 2011: Origin of the moisture feeding the heavy precipitating systems over southeastern France. *Nat. Hazards Earth Syst. Sci.*, **11**, 1163–1178, doi:10.5194/nhess-11-1163-2011.
- , and —, 2013: Assessment of the water supply to Mediterranean heavy precipitation: A method based on finely designed water budgets. *Atmos. Sci. Lett.*, **14**, 133–138, doi:10.1002/asl2.429.
- Frei, C., and C. Schär, 1998: A precipitation climatology of the Alps from high-resolution rain-gauge observations. *Int. J. Climatol.*, **18**, 873–900, doi:10.1002/(SICI)1097-0088(19980630)18:8<873::AID-JOC255>3.0.CO;2-9.
- Fresnay, S., 2014: Prévisibilité des épisodes météorologiques à fort impact: Sensibilité aux anomalies d'altitude (Predictability of high-impact weather events: Sensitivity to altitude anomalies). Ph.D. thesis, Université Paul Sabatier-Toulouse III, 200 pp. [Available online at [https://tel.archives-ouvertes.fr/tel-00986467/file/these\\_fresnay.pdf](https://tel.archives-ouvertes.fr/tel-00986467/file/these_fresnay.pdf).]
- Funatsu, B. M., C. Claud, and J.-P. Chaboureaud, 2008: A 6-year AMSU-based climatology of upper-level troughs and associated precipitation distribution in the Mediterranean region. *J. Geophys. Res.*, **113**, D15120, doi:10.1029/2008JD009918.
- , —, and —, 2009: Comparison between the large-scale environments of moderate and intense precipitating systems in the Mediterranean region. *Mon. Wea. Rev.*, **137**, 3933–3959, doi:10.1175/2009MWR2922.1.
- Giorgi, F., C. Jones, G. R. Asrar, 2009: Addressing climate information needs at the regional level: The CORDEX framework. *WMO Bull.*, **58**, 175–183. [Available online at [http://www.wmo.int/pages/publications/bulletinarchive/archive/58\\_3\\_en/documents/58\\_3\\_giorgi\\_en.pdf](http://www.wmo.int/pages/publications/bulletinarchive/archive/58_3_en/documents/58_3_giorgi_en.pdf).]
- Gladich, I., I. Gallai, D. B. Gaiotti, and F. Stel, 2011: On the diurnal cycle of deep moist convection in the southern side of the Alps analysed through cloud-to-ground lightning activity. *Atmos. Res.*, **100**, 371–376, doi:10.1016/j.atmosres.2010.08.026.
- Haylock, M. R., and C. M. Goodess, 2004: Interannual variability of European extreme winter rainfall and links with mean large-scale circulation. *Int. J. Climatol.*, **24**, 759–776, doi:10.1002/joc.1033.
- Hong, S.-Y., J. Dudhia, and S.-H. Chen, 2004: A revised approach to ice microphysical processes for the bulk parameterization of clouds and precipitation. *Mon. Wea. Rev.*, **132**, 103–120, doi:10.1175/1520-0493(2004)132<0103:ARATIM>2.0.CO;2.
- Kain, J. S., 2004: The Kain–Fritsch convective parameterization: An update. *J. Appl. Meteor.*, **43**, 170–181, doi:10.1175/1520-0450(2004)043<0170:TKCPAU>2.0.CO;2.
- Karagiannidis, A. F., A. A. Bloutsos, P. Maheras, and C. Sachsamanoglou, 2008: Some statistical characteristics of precipitation in Europe. *Theor. Appl. Climatol.*, **91**, 193–204, doi:10.1007/s00704-007-0303-7.
- Kömüşçü, A. M., 1998: Analysis of meteorological and terrain features leading to the Izmir flash flood, 3–4 November 1995. *Nat. Hazards*, **18**, 1–25, doi:10.1023/A:1008078920113.

- Landin, M. G., and L. F. Bosart, 1989: The diurnal variation of precipitation in California and Nevada. *Mon. Wea. Rev.*, **117**, 1801–1816, doi:[10.1175/1520-0493\(1989\)117<1801:TDVOPI>2.0.CO;2](https://doi.org/10.1175/1520-0493(1989)117<1801:TDVOPI>2.0.CO;2).
- Le Bouar, E., E. Moreau, and J. Testud, 2008: The rain accumulation product from the X-band polarimetric radar Hydrix. *Int. Symp. on Weather Radar and Hydrology*, Grenoble/Autrans, France, LTHE–OHMCV.
- Lemaître, Y., J.-F. Rysman, S. Verrier, and E. Moreau, 2013: Le radar en bande X: Un outil au service de l'étude des événements précipitants (X-band radar: A tool for studying precipitation events). *Meteorologie*, **83**, 50–58. [Available online at <http://documents.irevues.inist.fr/handle/2042/52054>.]
- Lin, C., S. Vasić, A. Kilambi, B. Turner, and I. Zawadzki, 2005: Precipitation forecast skill of numerical weather prediction models and radar nowcasts. *Geophys. Res. Lett.*, **32**, L14801, doi:[10.1029/2005GL023451](https://doi.org/10.1029/2005GL023451).
- Lionello, P., P. Malanotte-Rizzoli, and R. Boscolo, 2006: *Mediterranean Climate Variability*. Developments in Earth and Environmental Sciences, Vol. 4, Elsevier, 438 pp.
- Mandapaka, P. V., U. Germann, and L. Panziera, 2012: Diurnal cycle of precipitation over complex Alpine orography: Inferences from high-resolution radar observations. *Quart. J. Roy. Meteor. Soc.*, **139**, 1025–1046, doi:[10.1002/qj.2013](https://doi.org/10.1002/qj.2013).
- Mariotti, A., M. Vittoria Struglia, N. Zeng, and K.-M. Lau, 2002a: The hydrological cycle in the Mediterranean region and implications for the water budget of the Mediterranean Sea. *J. Climate*, **15**, 1674–1690, doi:[10.1175/1520-0442\(2002\)015<1674:THCITM>2.0.CO;2](https://doi.org/10.1175/1520-0442(2002)015<1674:THCITM>2.0.CO;2).
- , N. Zeng, and K.-M. Lau, 2002b: Euro-Mediterranean rainfall and ENSO—A seasonally varying relationship. *Geophys. Res. Lett.*, **29**, 1621, doi:[10.1029/2001GL014248](https://doi.org/10.1029/2001GL014248).
- Mlawer, E. J., S. J. Taubman, P. D. Brown, M. J. Iacono, and S. A. Clough, 1997: Radiative transfer for inhomogeneous atmospheres: RRTM, a validated correlated-k model for the longwave. *J. Geophys. Res.*, **102**, 16 663–16 682, doi:[10.1029/97JD00237](https://doi.org/10.1029/97JD00237).
- Moreau, E., J. Testud, and E. Le Bouar, 2009: Rainfall spatial variability observed by X-band weather radar and its implication for the accuracy of rainfall estimates. *Adv. Water Resour.*, **32**, 1011–1019, doi:[10.1016/j.advwatres.2008.11.007](https://doi.org/10.1016/j.advwatres.2008.11.007).
- Nastos, P., J. Kapsomenakis, and K. Douvis, 2013: Analysis of precipitation extremes based on satellite and high-resolution gridded data set over Mediterranean basin. *Atmos. Res.*, **131**, 46–59, doi:[10.1016/j.atmosres.2013.04.009](https://doi.org/10.1016/j.atmosres.2013.04.009).
- Nittis, K., C. Tziavos, R. Bozzano, V. Cardin, Y. Thanos, G. Petihakis, M. E. Schiano, and F. Zanon, 2007: The M3A multi-sensor buoy network of the Mediterranean Sea. *Ocean Sci.*, **3**, 229–243, doi:[10.5194/os-3-229-2007](https://doi.org/10.5194/os-3-229-2007).
- Noh, Y., W. Cheon, S. Hong, and S. Raasch, 2003: Improvement of the *k*-profile model for the planetary boundary layer based on large eddy simulation data. *Bound.-Layer Meteor.*, **107**, 401–427, doi:[10.1023/A:1022146015946](https://doi.org/10.1023/A:1022146015946).
- Nuissier, O., V. Ducrocq, D. Ricard, C. Lebeaupin, and S. Anquetin, 2008: A numerical study of three catastrophic precipitating events over southern France. I: Numerical framework and synoptic ingredients. *Quart. J. Roy. Meteor. Soc.*, **134**, 111–130, doi:[10.1002/qj.200](https://doi.org/10.1002/qj.200).
- Oki, T., and K. Musiak, 1994: Seasonal change of the diurnal cycle of precipitation over Japan and Malaysia. *J. Appl. Meteor.*, **33**, 1445–1463, doi:[10.1175/1520-0450\(1994\)033<1445:SCOTDC>2.0.CO;2](https://doi.org/10.1175/1520-0450(1994)033<1445:SCOTDC>2.0.CO;2).
- Orlanski, I., 1975: A rational subdivision of scales for atmospheric processes. *Bull. Amer. Meteor. Soc.*, **56**, 527–530.
- Panziera, L., and U. Germann, 2010: The relation between airflow and orographic precipitation on the southern side of the Alps as revealed by weather radar. *Quart. J. Roy. Meteor. Soc.*, **136**, 222–238, doi:[10.1002/qj.544](https://doi.org/10.1002/qj.544).
- , —, M. Gabella, and P. V. Mandapaka, 2011: NORA—Nowcasting of Orographic Rainfall by means of Analogues. *Quart. J. Roy. Meteor. Soc.*, **137**, 2106–2123, doi:[10.1002/qj.878](https://doi.org/10.1002/qj.878).
- Price, C., L. Stone, A. Huppert, B. Rajagopalan, and P. Alpert, 1998: A possible link between El Niño and precipitation in Israel. *Geophys. Res. Lett.*, **25**, 3963–3966, doi:[10.1029/1998GL900098](https://doi.org/10.1029/1998GL900098).
- Rebora, N., and Coauthors, 2013: Extreme rainfall in the Mediterranean: What can we learn from observations? *J. Hydrometeor.*, **14**, 906–922, doi:[10.1175/JHM-D-12-083.1](https://doi.org/10.1175/JHM-D-12-083.1).
- Ricard, D., V. Ducrocq, and L. Auger, 2012: A climatology of the mesoscale environment associated with heavily precipitating events over a northwestern Mediterranean area. *J. Appl. Meteor. Climatol.*, **51**, 468–488, doi:[10.1175/JAMC-D-11-017.1](https://doi.org/10.1175/JAMC-D-11-017.1).
- Rotunno, R., and J. B. Klemm, 1982: The influence of the shear-induced pressure gradient on thunderstorm motion. *Mon. Wea. Rev.*, **110**, 136, doi:[10.1175/1520-0493\(1982\)110<0136:TIOTSI>2.0.CO;2](https://doi.org/10.1175/1520-0493(1982)110<0136:TIOTSI>2.0.CO;2).
- , —, and M. L. Weisman, 1988: A theory for strong, long-lived squall lines. *J. Atmos. Sci.*, **45**, 463–485, doi:[10.1175/1520-0469\(1988\)045<0463:ATFSL>2.0.CO;2](https://doi.org/10.1175/1520-0469(1988)045<0463:ATFSL>2.0.CO;2).
- Rudolph, J. V., K. Friedrich, and U. Germann, 2011: Relationship between radar-estimated precipitation and synoptic weather patterns in the European Alps. *J. Appl. Meteor. Climatol.*, **50**, 944–957, doi:[10.1175/2010JAMC2570.1](https://doi.org/10.1175/2010JAMC2570.1).
- Rysman, J.-F., 2013: Caractérisation multi-échelles de la pluie et des processus associés dans l'Eurorégion Alpes-Méditerranée - De l'observation radar à la prévision (Multiscale characterization of precipitation and associated processes in the Alps-Mediterranean Euroregion—From radar observation to forecast). Ph.D. thesis, Université Pierre et Marie Curie, 258 pp. [Available online at <https://hal.archives-ouvertes.fr/tel-01119716>.]
- , S. Verrier, Y. Lemaître, and E. Moreau, 2013: Space-time variability of the rainfall over the western Mediterranean region: A statistical analysis. *J. Geophys. Res. Atmos.*, **118**, 8448–8459, doi:[10.1002/jgrd.50656](https://doi.org/10.1002/jgrd.50656).
- , C. Claud, J.-P. Chaboureaud, J. Delanoë, and B. M. Funatsu, 2016: Severe convection in the Mediterranean from microwave observations and a convection-permitting model. *Quart. J. Roy. Meteor. Soc.*, doi:[10.1002/qj.2611](https://doi.org/10.1002/qj.2611), in press.
- Sénési, S., P. Bougeault, J.-L. Chêze, P. Cosentino, and R.-M. Thepenier, 1996: The Vaison-La-Romaine flash flood: Mesoscale analysis and predictability issues. *Wea. Forecasting*, **11**, 417–442, doi:[10.1175/1520-0434\(1996\)011<0417:TFLRFF>2.0.CO;2](https://doi.org/10.1175/1520-0434(1996)011<0417:TFLRFF>2.0.CO;2).
- Silvestro, F., S. Gabellani, F. Giannoni, A. Parodi, N. Rebora, R. Rudari, and F. Siccardi, 2012: A hydrological analysis of the 4 November 2011 event in Genoa. *Nat. Hazards Earth Syst. Sci.*, **12**, 2743–2752, doi:[10.5194/nhess-12-2743-2012](https://doi.org/10.5194/nhess-12-2743-2012).
- Simmons, A., S. Uppala, D. Dee, and S. Kobayashi, 2007: ERA-Interim: New ECMWF reanalysis products from 1989 onwards. *ECMWF Newsletter*, No. 110, ECMWF, Reading, United Kingdom, 25–35.
- Skamarock, W., J. Klemm, J. Dudhia, D. Gill, and D. Barker, 2008: A description of the Advanced Research WRF version 3. NCAR Tech. Rep. NCAR/TN-475+STR, 113 pp. [Available online at [http://www2.mmm.ucar.edu/wrf/users/docs/arw\\_v3.pdf](http://www2.mmm.ucar.edu/wrf/users/docs/arw_v3.pdf).]
- Smirnova, T. G., J. M. Brown, and S. G. Benjamin, 1997: Performance of different soil model configurations in simulating ground surface temperature and surface fluxes. *Mon. Wea.*

- Rev., **125**, 1870–1884, doi:[10.1175/1520-0493\(1997\)125<1870:PODSMC>2.0.CO;2](https://doi.org/10.1175/1520-0493(1997)125<1870:PODSMC>2.0.CO;2).
- , —, —, and D. Kim, 2000: Parameterization of cold-season processes in the MAPS land-surface scheme. *J. Geophys. Res.*, **105**, 4077–4086, doi:[10.1029/1999JD901047](https://doi.org/10.1029/1999JD901047).
- Smith, R. B., Q. Jiang, M. G. Fearon, P. Tabary, M. Dörninger, J. D. Doyle, and R. Benoit, 2003: Orographic precipitation and air mass transformation: An Alpine example. *Quart. J. Roy. Meteor. Soc.*, **129**, 433–454, doi:[10.1256/qj.01.212](https://doi.org/10.1256/qj.01.212).
- Stéfanon, M., P. Drobinski, F. D. Andrea, C. Lebeaupin-Brossier, and S. Bastin, 2013: Soil moisture–temperature feedbacks at meso-scale during summer heat waves over western Europe. *Climate Dyn.*, **42**, 1309–1324, doi:[10.1007/s00382-013-1794-9](https://doi.org/10.1007/s00382-013-1794-9).
- Svensson, C., and D. Jakob, 2002: Diurnal and seasonal characteristics of precipitation at an upland site in Scotland. *Int. J. Climatol.*, **22**, 587–598, doi:[10.1002/joc.674](https://doi.org/10.1002/joc.674).
- Tapiador, F. J., and Coauthors, 2012: Global precipitation measurement: Methods, datasets and applications. *Atmos. Res.*, **104–105**, 70–97, doi:[10.1016/j.atmosres.2011.10.021](https://doi.org/10.1016/j.atmosres.2011.10.021).
- Testud, J., E. Le Bouar, E. Obligis, and M. Ali-Mehenni, 2000: The rain profiling algorithm applied to polarimetric weather radar. *J. Atmos. Oceanic Technol.*, **17**, 332–356, doi:[10.1175/1520-0426\(2000\)017<0332:TRPAAT>2.0.CO;2](https://doi.org/10.1175/1520-0426(2000)017<0332:TRPAAT>2.0.CO;2).
- , J. Lavabre, S. Diss, P. Tabary, and G. Scialom, 2007: Hydrix radar in FRAMEA—Evaluation of an X band polarimetric radar using a quasi-co located S band radar and a raingauge network. *Proc. Int. Symp. on X Band Weather Radar Network*, Tsukuba, Japan, National Research Institute for Earth Science and Disaster Prevention. [Available online at [http://www.novimet.com/download/Testud%20et%20al\\_Japan\\_2007.pdf](http://www.novimet.com/download/Testud%20et%20al_Japan_2007.pdf).]
- Vasić, S., C. A. Lin, I. Zawadzki, O. Bousquet, and D. Chaumont, 2007: Evaluation of precipitation from numerical weather prediction models and satellites using values retrieved from radars. *Mon. Wea. Rev.*, **135**, 3750–3766, doi:[10.1175/2007MWR1955.1](https://doi.org/10.1175/2007MWR1955.1).
- Walser, A., and C. Schar, 2004: Convection-resolving precipitation forecasting and its predictability in Alpine river catchments. *J. Hydrol.*, **288**, 57–73, doi:[10.1016/j.jhydrol.2003.11.035](https://doi.org/10.1016/j.jhydrol.2003.11.035).
- Weisman, M. L., and R. Rotunno, 2000: The use of vertical wind shear versus helicity in interpreting supercell dynamics. *J. Atmos. Sci.*, **57**, 1452–1472, doi:[10.1175/1520-0469\(2000\)057<1452:TUOVWS>2.0.CO;2](https://doi.org/10.1175/1520-0469(2000)057<1452:TUOVWS>2.0.CO;2).
- Wüest, M., C. Frei, A. Altenhoff, M. Hagen, M. Litschi, and C. Schär, 2010: A gridded hourly precipitation dataset for Switzerland using rain-gauge analysis and radar-based disaggregation. *Int. J. Climatol.*, **30**, 1764–1775, doi:[10.1002/joc.2025](https://doi.org/10.1002/joc.2025).